COMPARISON OF USING AIR, CO_2 AND HELIUM FOR THE COOLING OF SQUARE-SHAPED ELECTRONIC PARTS: CFD STUDY WITH ENTROPY GENERATION ANALYSIS

***Mohamed A. KARALI*[1]*, Bandar Awadh ALMOHAMMADI*[2]*, Abdullah M. A. ALSHARIF*[2]*, Kaveri Umesh KADAM*[3]*, Abdul KHALIQ*[2]*, Hassanein A. REFAEY*[2,4*]*, Eslam HUSSEIN*[4]**

[1]Department of Mechanical Engineering, Faculty of Engineering and Technology, Future University in Egypt, New Cairo, Egypt

[2]Department of Mechanical Engineering, College of Engineering at Yanbu, Taibah University, Yanbu Al-Bahr 41911, Saudi Arabia

[3]Department of Computer Science & Engineering, School of Engineering Sciences and Technology, Jamia Hamdard, New Delhi-110062, India

[4]Department of Mechanical Engineering, Benha Faculty of Engineering, Benha University, Benha, 13511, Egypt

[*] Corresponding authors; Email: hassanein.refaey@feng.bu.edu.eg

Numerical simulation has been used in the current work to investigate improving the cool-down of electronic parts of cubical form involving dummy parts within a rectangular duct. Three working fluids (Air, CO2, and Helium) were used to cool 12 electrical chip arrays in the duct. The simulation investigates the effects of cooling fluid type and shifting hot element placements on whole cooling functioning at various Reynolds numbers. Also, the impact of the distance among electronic parts is researched. This is accomplished by moving the heat sources while leaving other components in their original positions as dummies to preserve the flow characteristics. The Reynolds number, Re, falls between (500 to 19000). The dimensionless entropy generation number reduces with the rise of the Re, while the pumping power ratio increases. It is determined that the dimensionless entropy generation computed for the case of constant viscosity of air yields slightly greater values than those obtained for the case of temperature-dependent viscosity. A high level of agreement in the experimental work is used to verify the standard k-model.

Key words*: Entropy generation; Electronic component cooling; Heat Source; CFD numerical simulation*

1. Introduction

The high operating temperature of electronic devices such as laptops, cell phones, and digital cameras is one of the main causes that damage their components. The operating temperature increases to critical value due to the devices' limited size, design, and mechanical speed because of improved processing speed design and shrinking of such devices' sizes. As a result, more heat is generated,

raising the working temperature to unsafe levels over the critical limitations. It is crucial to optimize the cooling process since the breakdown rate of these devices is absolutely related to the operating temperature. Therefore, improving the cooling process is essential to avoid high heat generation [1]. In literature, many researchers have dealt with improving the cooling of electronic devices [1-6]. There are three methods to improve the cooling process: enhancing the surface area of electronic components (fin or pin surface), using phase change materials (PCM), and improving thermal conductivity, spacing, and flow rates of working coolant [7-10]. The effectiveness of cylindrical lithium-ion battery cooling devices was quantitatively examined by Behrooz et al. [11]. This research concentrated on the cooling system's intake and outlet and battery distance impact. The results demonstrated that the input size and *Re* change affected the operating temperature and pressure. Selvan and Manavalla [12] used two types of PCM materials, OM35 (50:50) and OM35 (60:40) for cooling E-machine. Three configurations were numerically created to study the thermal behavior of brackets during the cooling process. The outcomes demonstrated that high heat was transferred with increasing spacing between the brackets.

The use of nanofluid as a new coolant with a mini channel for downsizing electronic components was also presented in a review by Bahiraei and Heshmatian [13]. Bahiraei and Monavari [14] investigated the influence of irregularly shaped nanoparticles in a microchannel heat sink at varying Reynolds numbers. The results showed the lowest heat resistance for the platelet particle-containing suspension. Greiner [15] showed that slow recirculation in channeled regions minimizes convective heat transfer, revealing diffusion as the primary mode of heat transfer. A numerical analysis for cooling a heat sink made of triangular pins was given by Alam et al. [16]. According to the findings, raising the air velocity raised the Nusselt number (*Nu*), improving heat removal from the CPU. Ali et al. [17] analyzed experimental and numerical data when considering the impact of distance between two-element heat sources. They demonstrated relationships between the Nusselt number and the package spacing with *Re* value ($2,464.6 \leq Re_L \leq 16,430$). The features of heat transmission in grooved channels were given by Farhanieh et al. [18]. The results showed that the pace at which heat was transferred from heated components was significantly affected by the degree to which the flow was reattached and recirculated. When grooved channels were compared to flat channels, the findings revealed a 300% improvement in heat transmission. Asako and Faghri [19] simulated the laminar and turbulent flows with a localized heat flux for a heated arrangement block. The outcomes revealed that transportation in dense arrays was more effective when approaching from above.

Molki and Fagri [20] described the forced convection of air-cooled rectangular blocks in a line. Nakayama and Park [21] investigated conjugated heat transfer from an airflow-mounted rectangular block. Laminar mixed convection heat transport in a quadrilateral channel was studied quantitatively by Kurşun and Sivriolu [22]. Bahiraei et al. [23] numerically studied the elliptical pin-fin heat sink while employing silver–water nanofluids for cooling. Bahiraei and Mazaheri [24] have tested spiral liquid blocks with nanoplatelets made of graphene to cool electronic devices. The spiral liquid block's heat transmission was excellent and energy efficient.

A theoretical and experimental examination was carried out by Refaey et al. [1 and 2] to enhance the heat transmission from 12 cubical heat sources within a quadrilateral duct. This research investigated how heat transmission is affected by the element spacing and the cooling air flow rate. Only two heat source components were explored using CFD and experiments; the rest were dummy

elements to maintain flow characteristics, with Re_L ranging from 4,108 to 17,115. At a Re_L value of 8,538, the most distant second heat source boosted the efficiency of the first upstream heat source by 17% and 10%, respectively. When all elements in the array were heated and compared to only two heat elements, a maximum reduction of approximately 19% and 15% in average Nusselt number for an in-line and lateral position was obtained when the second heat element was located at positions 8 and 4, respectively, at Re =17,115. This was found after heating all of the array's elements. Several papers [25-29] examined the working fluid (single phase or nanofluids), entropy creation, and heat transfer enhancement.

Since the experimental work on this topic is tough for large ranges of Re, the current study was planned to present numerous numerical CFD simulations for an extensive range of Re_L from 500 to 19000. The current article examines various factors, such as the cooling fluid employed (three different working fluids are used), the distance between heat sources, and the flow velocity of the cooling fluid. As a result, a total of 165 cases in the present study involving the position of heat sources were analyzed. The cooling efficiency as a function of the heat source placement is studied. In addition, an entropy generation was analyzed for the studied cases.

2. Numerical analysis

The computational domain simulates the cooling airflow through or across an array of rectangular parts demonstrating electronic components (chips 3×4) on a circuit board. The simulation examines how altering hot component placements affects cooling performance at various Re values and the impact of electronic component spacing. Changing positions strategy: all blocks with heat (on), one block (the specified ones) without heat that is deemed a dummy element to retain flow characteristics, and two or three components without heat in the same inline distinguished plane. Creating 11 runs for each Re value (five points), totaling 165 cases. Figures 1 (a), (b), and (c) show the computational domain test section information. Chip domains are twelve rectangular metal blocks (3 columns × 4 rows). The first row is 500 mm from the duct entry and at the bottom to provide fully established flow conditions.

The computational domain generates a three-dimensional uniform volume mesh. The domain uses tetrahedron components, whereas the chips domain uses structured elements. A tiny mesh near the chip walls with the dimensionless y + maximum consequence of 1.0 eliminates the boundary layer's influence on CFD results; this can be shown in Figures 1 (d) and (e). Boundaries are fluid input velocity at the inlet according to Re_L values containing five points: 500, 1000, 5000, 13000, and 19000, inlet temperature 300 K, pressure outlet at the outlet, adiabatic duct walls, and chips bottom walls. 140000 W/m^3 (3.5 W) is the heat production of each heat source. Refaey et al. [2] recommended the standard κ–ε turbulence model with a turbulence intensity of 5% to be the best model among other used models that describe the presently studied problem.

The calculated parameters heat flux, q, average heat transfer coefficient, h, Reynolds, Re_L, and average Nusselt number, Nu_L are presented in [17], are as follows:

$$q=\frac{Q_{net}}{A_s} \text{ (1)}, \quad \square = \frac{q}{T_m - T_i} \text{ (2)}, \quad Re_L = \frac{vL}{\upsilon} \text{ (3)}, \quad Nu_L = \frac{\square L}{k} \text{ (4)}$$

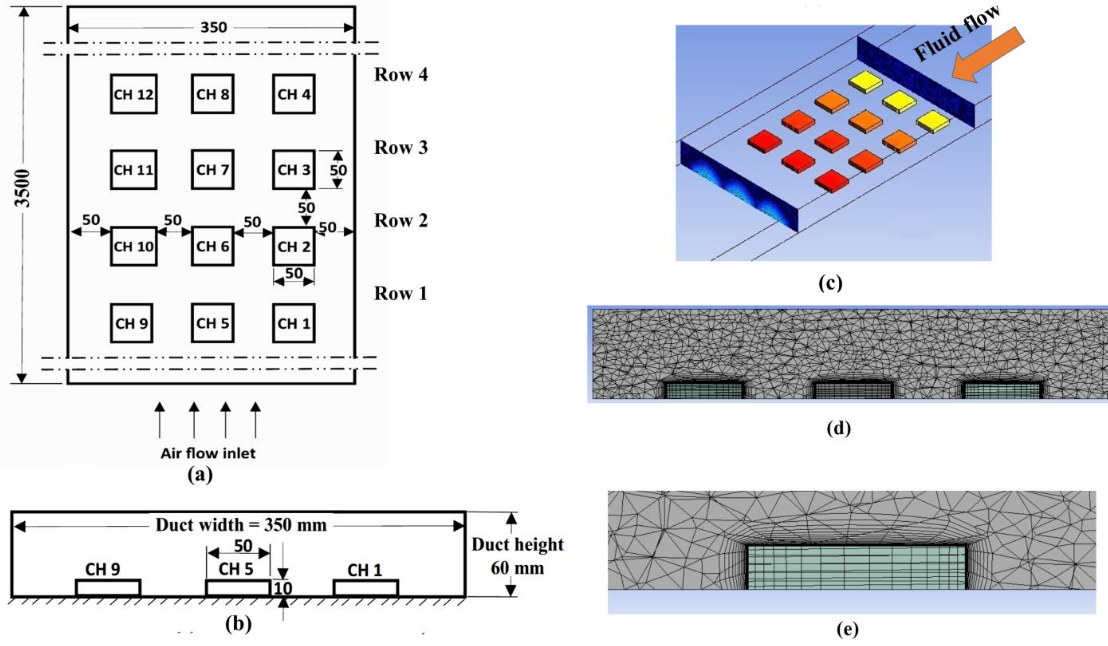

Figure 1. Details description of CFD domain (a) Specifies view (b) Sectional view (c) CFD domain (d) Mesh details (e) Mesh zoom-in view

Cartesian coordinates are used by Ali et al. [17] to solve continuity, momentum, and energy equations to determine temperature distribution, flow field, and heat transfer in the duct. The existing model's solution converged when continuity, momentum, and energy residuals approached 10^{-4}, 10^{-6}, and 10^{-7}. Five sets of grids are used to verify mesh independence, including the number of cells: 320,805, 413,187, 558,128, 771,436, and 931,553. Based on the average surface temperature of chips 5, 6, 7, and 8 at $Re_L = 5000$, a mesh independence test was performed. It was found that, when starting to use the grid with cells number 558,128 and so on the afterwise grids, a minimal effect on temperature changes was recorded with an average deviation value of 0.006%. Hence, the grid with cell numbers 558,128 is utilized for all cases in this work [1].

$$\nabla.(\rho U) = 0 \tag{5}$$

$$\nabla.(\rho UU) = -\nabla P + \nabla.[\mu_t(\nabla U + \nabla U^T)] \tag{6}$$

$$\nabla.\left(-\mathrm{k}\nabla \mathrm{T} + \rho C_p T U\right) = S_h \tag{7}$$

Where S_h is the thermal source term.

The validation of the current numerical model can be found in Refaey et al. [1]. This validation was conducted for air with the experimental data available from Refaey et al. [2] of heat energy produced by a single chip located in place 5 (referred to as a single heat source, SHS) or by two chips situated in places 5 and 6, respectively for *Re* between 3611 and 14174. The validation results showed an average difference of 14.6% between numerical and experimental data.

3. Analysis of entropy generation and pumping power

Considering the array of chips as a rectangular duct, as shown below, the entropy generation during heat transfer from chips to air flows in the duct is computed. A constant viscosity situation and a temperature-dependent air viscosity case are both explored. When doing this study, all active chips are used as the heat transfer source. An average heat transfer coefficient is used to transport heat to

most of the fluids. Since air is the most prevalent fluid used in these applications, only air underwent analysis. For various Reynolds numbers, the entropy production and pumping power are evaluated.

The rate of heat transfer to the flowing fluid of the control volume may be shown as

$$\delta\dot{Q} = \dot{m}C_p dT = \bar{h}\pi D(T_w - T)dx \tag{8}$$

The second law applied to the duct considered gives.

$$\dot{S}_{gen} = \frac{\delta S}{\delta t} - \frac{\dot{Q}}{T} + \sum_{out}\dot{m}s - \sum_{in}\dot{m}s \geq 0 \tag{9}$$

Considering air as a pure substance, the Canonical relation may be expressed as

$$\frac{dh}{dx} = T\frac{dh}{dx} + \frac{1}{\rho}\frac{dh}{dx} \tag{10}$$

Using the Canonical relation, the generation of entropy rate may be expressed as

$$d\dot{S}_{gen} = \dot{m}C_p\left(\frac{T_w - T}{T_w T}dT - \frac{1}{\rho C_p T}dp\right) \tag{11}$$

It may further be expressed as

$$d\dot{S}_{gen} = \dot{m}C_p\left(\frac{T_w - T_i}{T_w T}e^{\frac{-4S_t x}{D}}dT + \frac{f\bar{U}^2}{2C_p dT}dx\right) \tag{12}$$

Integrating the above equation along the duct length, the entropy generation can be shown as

$$\dot{S}_{gen} = \dot{m}C_p\left[\ln\left(\frac{1 - \alpha e^{-4S_t\emptyset}}{1 - \alpha}\right) - \alpha\left(1 - e^{-4S_t\emptyset}\right) + \frac{f\alpha E_c}{8S_t}\ln\left(\frac{e^{4S_t\emptyset} - \alpha}{1 - \alpha}\right)\right] \tag{13}$$

It is possible to calculate the dimensionless entropy generation, which is the ratio of entropy generation per unit of heat transport, as

$$N = \frac{1}{1 - e^{-4S_t\emptyset}} \times \left\{\ln\left(\frac{1 - \alpha e^{-4S_t\emptyset}}{1 - \alpha}\right) - \alpha\left(1 - e^{-4S_t\emptyset}\right) + \frac{1}{8}\left(\frac{64}{R_e}\right)\frac{\alpha E_c}{S_t}\ln\left(\frac{e^{4S_t\emptyset} - \alpha}{1 - \alpha}\right)\right\} \tag{14}$$

For a fully developed flow under laminar conditions and for the constant viscosity, the friction factor (*f*) is related to the *Re* as *f*= 64/*Re*

For the case of constant viscosity, dimensionless entropy generation may be obtained below.

$$N = \frac{1}{1 - e^{-4S_t\emptyset}} \times \left\{\ln\left(\frac{1 - \alpha e^{-4S_t\emptyset}}{1 - \alpha}\right) - \alpha\left(1 - e^{-4S_t\emptyset}\right) + 8\alpha\frac{E_c}{R_e S_t}\ln\left(\frac{e^{4S_t\emptyset} - \alpha}{1 - \alpha}\right)\right\} \tag{15}$$

The following relation may be employed to investigate the case of temperature-dependent viscosity of air for the computation of dimensionless entropy generation and pumping power ratio.

$$\frac{\mu}{\mu_0} = \left(\frac{T}{T_0}\right)^{3/4} \tag{16}$$

Where $\mu_0 = 1.82 \text{ x } 10^{-5}\ Pa.s$ at $T_0 = 291\ K$

$$dp = -\frac{32\bar{U}}{D^2}\left[\mu_0\left(\frac{T}{T_0}\right)^{3/4}\right]dx \tag{17}$$

$$\dot{S}_{gen} = \dot{m}C_p\left\{\left(\ln\left(\frac{1 - \alpha e^{-4\psi_1}}{1 - \alpha}\right) - \alpha\left(1 - e^{-4\psi_1}\right)\right) + \frac{32}{3}\frac{\bar{U}\mu_0}{\rho C_p D S_t T_0^{3/2}}\left((1 - \alpha e^{4\psi_1})^{3/4} - (1 - \alpha)^{3/4} + 3\psi_1\right)\right\} \tag{18}$$

$$N = \frac{1}{1 - e^{-4\psi_1}}\left\{\left(\ln\left(\frac{1 - \alpha e^{-4\psi_1}}{1 - \alpha}\right) - \alpha\left(1 - e^{-4\psi_1}\right)\right) + \frac{32}{3}\frac{\lambda}{S_t}\left((1 - \alpha e^{4\psi_1})^{3/4} - (1 - \alpha)^{3/4} + 3\psi_1\right)\right\} \tag{19}$$

Where $\lambda = \frac{\bar{U}\mu_0}{\rho C_p D T_0^{3/2}}$

$$P_r = \frac{32\phi}{\rho C_p D(T_w - T_i)(1 - e^{-4\psi_1})}\left[\mu_0\left[\frac{T_w(1 - e^{-4\psi_1})}{T_0}\right]^{3/4}\right] \quad (20)$$

$$P_r = \frac{32E_c\psi_1}{(1 - e^{-4\psi_1})}\xi\left[\frac{T_w(1 - e^{4\psi_1})}{T_0}\right]^{3/4} \quad (21)$$

Where $\xi = \frac{\mu_0 D}{3.66k\bar{U}}$

Further details of the abovementioned equations can be found in Ref. [30].

4. Results and discussions

4.1. One chip is a dummy element

Figure (2) shows the Nusselt number of chips 5 and 8 when one of the rest chips in its column (column 2) is a dummy and the rest are heat sources. It is possible to deduce from figure (2-a) that transferring the dummy block in the identical column from chip 5 has no effect on the Nusselt number for the three working fluids at all studied Reynolds numbers. On the other hand, regarding the *Nu* number for chip 8, the *Nu* number slightly increases as the dummy element is transferred toward chip 8 at the same *Re*. But this effect increases as the operating fluid changes and extreme enhancement is obtained using CO_2. This is attributed to two products, the first one is that as the dummy element is near chip 8, the chip's temperature decreases: consequently, *Nu* increases. The maximum growth in chip 5 *Nu* number reaches 10% at Re_L 5000 when using CO_2 instead of air. While for chip 8, the maximum increase in *Nu* number reaches 20% at Re_L 5000 when using CO_2 instead of air. This is mostly due to an increase in spacing between the focus on chip (chip 8) and the preceding heat source, which influences the cooling rate. In other words, when the dummy element is far away, chip 8 achieves its lowest *Nu* number for all Reynolds numbers. This indicates that there should be a gap between the two viewpoint chips for a high cooling rate.

Figure (3-a) shows temperature contours in isometric view and flow wise direction view for the case of only chip 5 is dummy when using CO_2 at Re_L = 19000. While Figure (3-b) shows the temperature change of chip 8 for the three working fluids when the fake element is moved through its column. One may infer that the temperature of chip 8 decreases at the same *Re* when the fake element is moved from chip 5 to chip 8 in the same column. As an example, chip 8 temperature at Re_L 5000 reached 331.57 K when chip 5 was a dummy and 307.1 *K* when chip 8 itself was a dummy while utilizing air. When chip 5 is a dummy, chip 8's temperature for CO_2 is 349 *K*, and when chip 8 is a dummy, it is 311 *K*. This is mainly caused by an increase in the distance between the target chip (chip 8), which impacts the cooling rate, and the prior heat source. In other words, chip 8 reached its highest temperature for all *Re* values when the fake element was distant from it. This indicates that a space between the two viewpoint chips is necessary for a high cooling rate. The velocity contours for the case of chip 5 is dummy is depicted in Figure (3-c) at Re_L = 19000 when using CO_2.

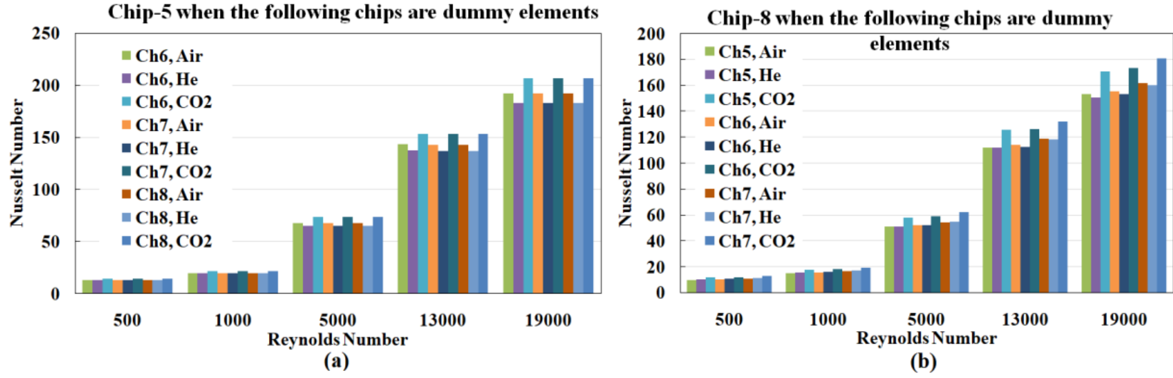

Figure 2. Variation of one chip Nusselt number with ReL on the same columns (a) chip 5 (b) chip 8

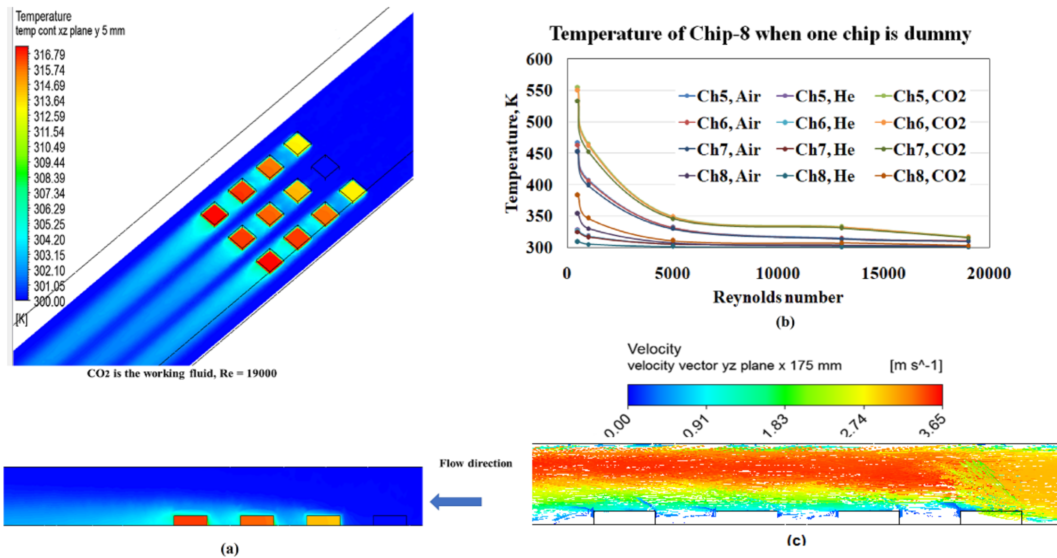

Figure 3. Sample of temperature results for one chip is dummy (a) Temperature contours, chip 5 is dummy, Re = 19000 for CO_2 (b) Variation of the chip 8 temperature with the three working fluids (c) Velocity contours, chip 5 is dummy, Re = 19000 for CO_2

4.2. Two chips are dummy elements

Figure (4) illustrates part of the findings as two chips are dummies, and the rest are used as heat sources. It depicts the relationship between chip 8 and chip 7 Nusselt number and Re_L. The figure revealed that as the flow inlet velocity increases, the airflow and recirculation flow side combination improve, and the Nu number increases linearly for the three working fluids. Furthermore, CO_2 gives a higher value for the two chips. This is attributed to the cooling effect of CO_2 being higher than air. When the input flow velocity rises, the temperatures of the two heat sources drop. At a higher input velocity, Figure (4) shows flow impingement on the second fake element (chip 6). Figure (5) shows temperature contours from sample cases for two chips are dummies, and the rest chips are heat sources, for the case of using CO_2 at Re = 19000.

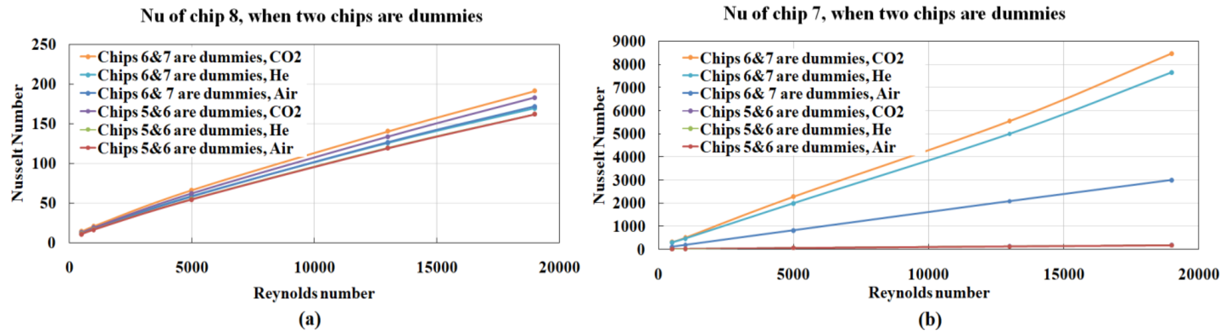

Figure 4. Sample cases of two chips are dummies, and the rest chips are heat sources (a) chip 8 (b) chip 7

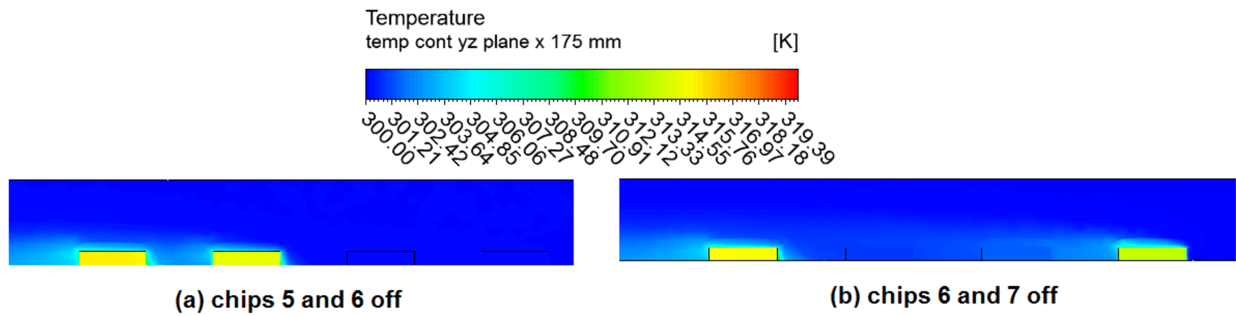

Figure 5. Temperature contours sample cases of two chips are dummies, and the rest chips are heat sources, for CO_2 at Re = 19000 (a) chips 5 and 6 (b) chips 6 and 7

4.3. Case of one row is a dummy

Figure 6 illustrates the findings when one row is a dummy, and all other chips are heat sources. The figure represents the Nu number values for chip 7 and chip 8 for the three working fluids at all Re_L. According to figure 6, the outcomes demonstrate that the trends are the same for all results whenever the dummy row position changes. Moreover, the Nu increases rapidly as the dummy row position is near the target chip. This is attributed to the reduction in chip temperature as the dummy row goes toward the chip. In addition, when the flow input velocity increases, the side blend of airflow and recirculation flow improves after the first row. The outcomes revealed an enhancement of 35% for chip 6 Nusselt number when using CO_2 instead of air when the second row is a dummy. This is attributed to the thermal conductivity of CO_2, which is lower than that of air. Furthermore, the final row temperatures rise because it stays a source term, and the flow transfers heat from prior rows and freezes a little quantity of warmness from it. The increase in distance between the chips in the final row and the preceding heat source (due to forming row 3 as a dummy) influences the cooling rate. Figure (7) shows temperature contours from sample cases of one row is dummy, and the rest chips are heat sources, for CO_2 at Re = 19000 (a) first row, (b) second row, (c) third row.

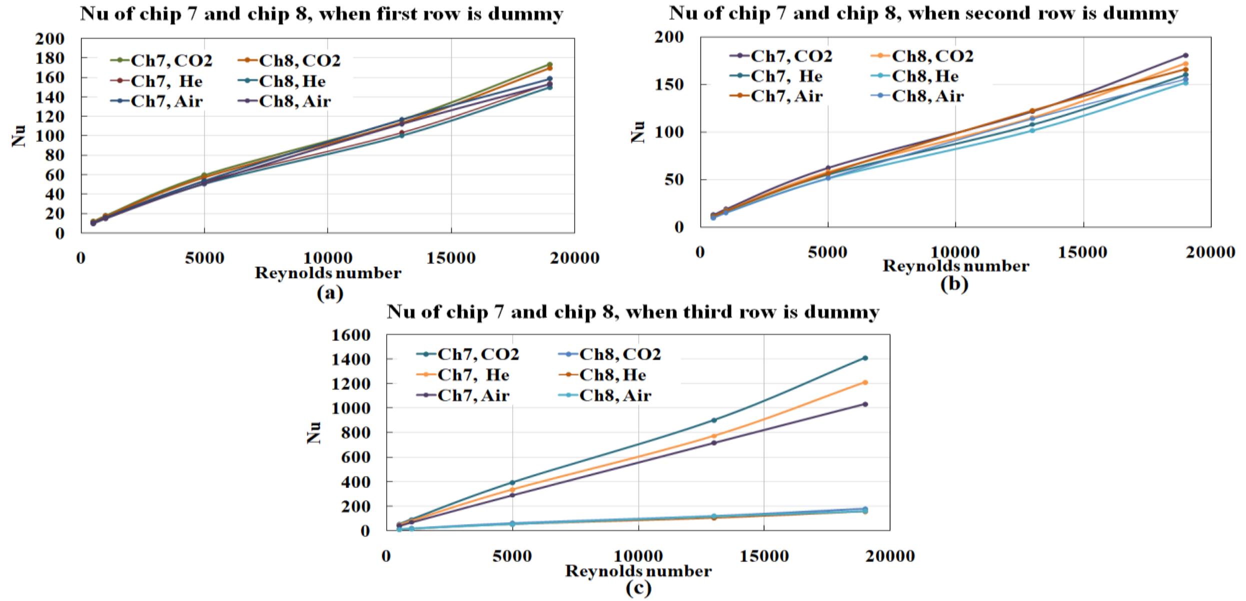

Figure 6. Sample cases of one row are dummies, and the rest chips are heat sources (a) first row, (b) second row, (c) third row

4.4. Entropy generation results

Fig. 8 (a) depicts the impact of the variation of Reynolds number on entropy generation during heat transfer to constant viscosity air flows in the rectangular duct. A dimensionless parameter is termed an entropy generation number. Since the friction factor f reflects the reciprocal of the Re, the dimensionless entropy generation number N, defined as the ratio of entropy created to the total heat transfer rate to the duct, is observed to decrease with an increase in Re. The pumping power to heat transfer rate ratio, defined in Fig. 8 (b) as the relationship between the parameter Pr and the fluctuation in the Re, is shown to increase as the Re rises. This is because the promotion of Re leads to an increase in the product of flow velocity and equivalent diameter of the rectangular duct, which appears in the numerator of expression obtained to compute the Pr for constant viscosity air flow in the duct.

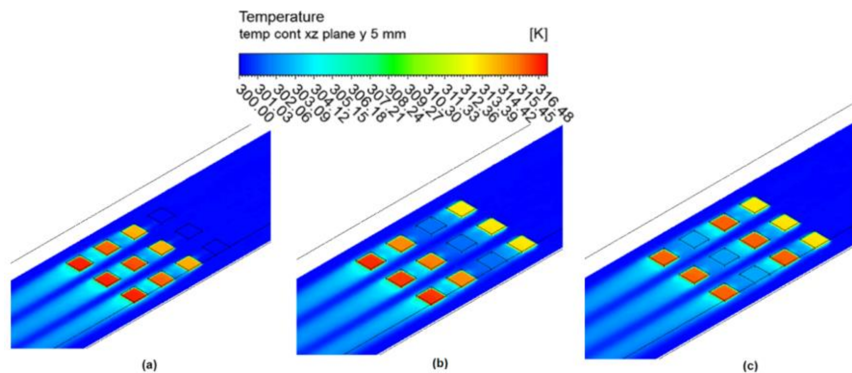

Figure 7. Temperature contours from sample cases of one row is dummy, and the rest chips are heat sources, for CO_2 at *Re* = 19000 (a) first row, (b) second row, (c) third row

ig. 9 (a) demonstrates the impact of the change of *Re* on entropy generation during heat transfer to temperature-dependent viscosity air flows in the rectangular duct. Since the viscosity of air is minimal, the quantities of *N* entropy generation number show decreasing behavior like the constant viscosity case of Fig. 8 (a). Furthermore, it is shown that the dimensionless entropy generation *N* estimated for constant viscosity gives somewhat greater values than those found for temperature-dependent viscosity. Figure 9 (b) depicts the effect of *Re* change on the pumping power to heat transfer rate ratio *Pr* for the temperature-dependent viscosity example of airflow. A significant rise in the values of *Pr* is observed with the more extensive promotion of the *Re*, which is found due to an increase in bulk temperature and viscosity. The temperature-dependent viscosity assumption values for *Pr* are lower than those of *Pr* obtained for the constant viscosity case.

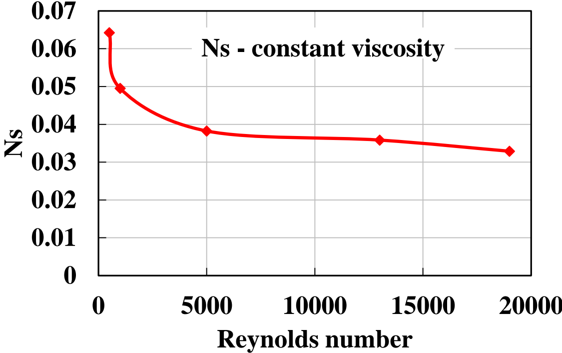

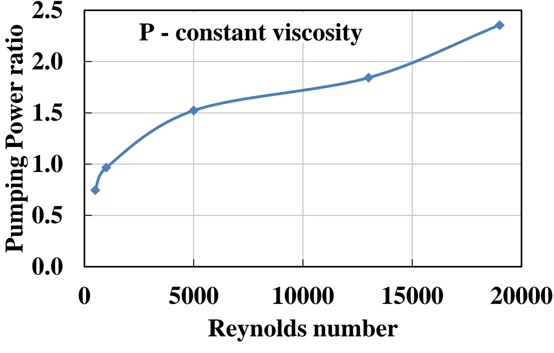

Figure 8 (a). Impact of the variation of Reynolds number on dimensionless entropy generation rate for constant viscosity air flow

Figure 8 (b). Impact of the variation of Reynolds number on pumping power to heat transfer for constant viscosity air flow

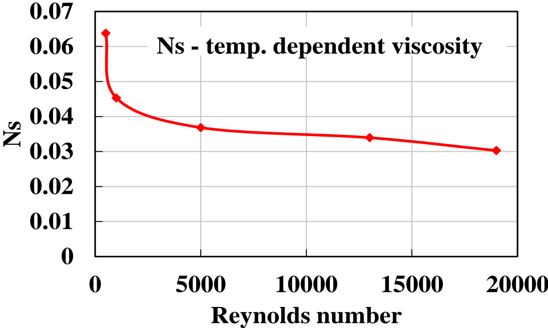

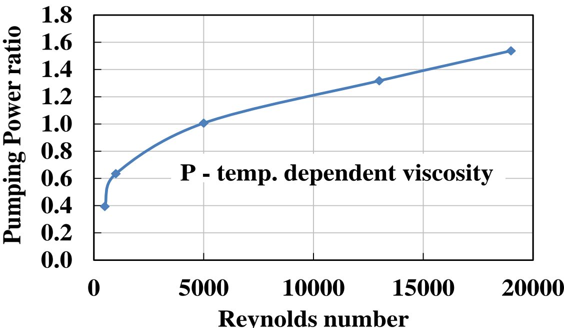

Figure 9 (a). Impact of the variation of Reynolds number on dimensionless entropy generation for temperature dependent viscosity air flow

Figure 9 (b). Impact of the variation of Reynolds number on pumping power to heat transfer rate temperature dependent viscosity air flow

5. Conclusions

This work displays a sizable numerical simulation that was run to look at ways to increase the cooling of false and cubic electronics pieces within a rectangular duct. Furthermore, because of difficulties in executing experiments to obtain low values of Reynolds number, the current study

provides CFD simulations with minimal Reynolds number of 500.12 electrical chips (3 × 4 array) are tested in an air duct across a wide range of Re_L, from 500 to 19000. The study focuses on the effect of adjusting the cooling airflow rate and chip spacing on cooling improvement. To do this, the following points are detected while the heat sources are shifted, and the remaining components are used as dummies to retain the flow characteristics:

- Increasing the inflow flow rate lowers the temperatures of the chips for all working fluids.

-The impact of Re_L on the resultant temperature is significantly more significant when $Re_L < 500$, reduced when $5000 < Re_L < 10000$, and minor when $Re_L > 10000$.

-The elements farthest away from the duct inlets had the most excellent temperatures when the dummy element was far from it.

- The cooling rate is adjusted by increasing the space between components in the fluid flow direction.

- Designers should run such electronic board systems at optimized higher Re_L levels and with CO_2 as an operating fluid.

- An enhancement of 35% for chip 6 Nusselt number when CO_2 is used instead of air while the second row is a dummy.

-Increasing the *Re* resulted in decreasing the dimensionless entropy generation number.

- The pumping power ratio is observed to be increasing with the promotion of the *Re*.

- The calculated findings show that dimensionless entropy generation computed for the case of constant viscosity of air provides somewhat higher values than dimensionless entropy generation computed for the case of temperature-dependent viscosity. The analysis carried out using the equations formulated for dimensionless entropy generation number and pumping power ratio is limited to the conditions of laminar flow of fluid through a duct of constant surface temperature.

Nomenclature

Symbols

As	heat element surface area, [m^2]
h	convection heat transfer coeff., [$Wm^{-2}K^{-1}$]
k	thermal conductivity, [$Wm^{-1}K^{-1}$]
L	heat source length, [m]
Q	heat transfer rate, [W]
q	heat flux, [W/m^2]
T	temperature, [K]
v	mean velocity, [m/s]
L	based on chip length
m	mean
net	The net amount of heat

Dimensionless groups

Nu	average Nusselt number $(=\frac{\square L}{k}), [-]$
Re	Reynolds number $(=\frac{vL}{\upsilon}), [-]$

Greek letters

ν	kinematic viscosity, [m^2/s]

Abbreviations

avg	average
CFD	Computational Fluid Dynamics
CH	chip
CPU	Central processing unit
max	maximum
min	minimum
PCM	phase change material
RANS	Reynolds Averaged Navier-Stokes
SHS	single heat source
temp	temperature

Subscripts

1:12	chips numbers
a	air
i	inlet

References

[1] Farzaneh, M., *et al.,* Design of Bifurcating Microchannels With/Without Loops for Cooling of Square-Shaped Electronic Components, *Applied Thermal Engineering*, *108* (2016), pp. 581–595, doi:10.1016/j.applthermaleng.2016.07.099

[2] Refaey, H. A., *et al.*, Cooling Enhancement of Cubical Shapes Electronic Components Array Including Dummy Elements Inside a Rectangular Duct, *Thermal Science*, *27* (2022), 2B, pp. 1529-1538, doi:10.2298/tsci220523134r

[3] Refaey, H. A., *et al.*, Numerical and Experimental Study for Heat Transfer Enhancement of Cubical Heat Source and Dummy Elements inside Rectangular Duct, *Warme- und Stoffubertragung [Heat and Mass Transfer], 57* (2021), 8, pp. 1319–1328, doi:10.1007/s00231-021-03033-w

[4] Bensafi, M., *et al.*, Experimental Investigation of Cooling Performance in Electronic instruments, *Thermal Science*, *27* (2023), 4B, pp. 3445-3455

[5] Zhang, Y., *et al.*, Theoretical Calculation and Simulation of Surface-Modified Scalable Silicon Heat Sink for Electronics Cooling, *Thermal Science*, *25* (2021), 6A, pp. 4181–4187, doi:10.2298/tsci2106181z

[6] Ma, Y., *et al.*, Performance Study on a Printed Circuit Heat Exchanger Composed of Novel Airfoil Fins for Supercritical CO_2 Cycle Cooling System, *Thermal Science*, *27* (2023), 1B, pp. 891–903, doi:10.2298/tsci220408112m

[7] Kumar, A., *et al.,* Thermal Performance of Heat Sink Using Nano-Enhanced Phase Change Material (NePCM) for Cooling of Electronic Components, *Microelectronics and Reliability*, *121* (2021), p. 114144, doi:10.1016/j.microrel.2021.114144

[8] Tauseef-Ur-, R., and Ali, H. M., Experimental Study on the Thermal Behavior of RT-35HC Paraffin within Copper and Iron-Nickel Open Cell Foams: Energy Storage for Thermal Management of Electronics, *International Journal of Heat and Mass Transfer, 146* (2020), p. 118852, doi:10.1016/j.ijheatmasstransfer.2019.118852

[9] Baby, R., and Balaji, C., Experimental Investigations on Phase Change Material Based Finned Heat Sinks for Electronic Equipment Cooling, *International Journal of Heat and Mass Transfer, 55*, (2012), 5-6, pp. 1642–1649, doi:10.1016/j.ijheatmasstransfer.2011.11.020

[10] Arshad, A., *et al.,* Experimental Investigation of PCM Based Round Pin-Fin Heat Sinks for Thermal Management of Electronics: Effect of Pin Fin Diameter, *Int. J. Heat Mass Transf, 117* (2018), pp. 861–872

[11] Behrooz, R., *et al.,* Numerical Simulation of the Effect of Battery Distance and Inlet and Outlet Length on the Cooling of Cylindrical Lithium-Ion Batteries and Overall Performance of Thermal Management System, *Journal of Energy Storage, 45* (2022), p. 103714, doi:10.1016/j.est.2021.103714

[12] Selvan, J., and Manavalla, S., Numerical Analysis of E-Machine Cooling Using Phase Change Material, *Energies, 15* (2022), 15, p. 5594, doi:10.3390/en15155594.

[13] Bahiraei, M., and Heshmatian, S., Electronics Cooling with Nanofluids: A Critical Review, *Energy Conversion and Management, 172* (2018), pp. 438–456, doi:10.1016/j.enconman.2018.07.047

[14] Bahiraei, M., and Monavari, A., Impact of Nanoparticle Shape on Thermohydraulic Performance of a Nanofluid in an Enhanced Microchannel Heat Sink for Utilization in Cooling of Electronic Components, *Chinese Journal of Chemical Engineering, 40* (2021), pp. 36–47, doi:10.1016/j.cjche.2020.11.026

[15] Greiner, M., An Experimental Investigation of Resonant Heat Transfer Enhancement in Grooved Channels, *International Journal of Heat and Mass Transfer, 34* (1991), 6, pp. 1383–1391, doi:10.1016/0017-9310(91)90282-j

[16] Alam, M. W., *et al.,* CPU Heat Sink Cooling by Triangular Shape Micro-Pin-Fin: Numerical Study, *International Communications in Heat and Mass Transfer, 112* (2020), p. 104455, doi:10.1016/j.icheatmasstransfer.2019.104455

[17] Ali, R. K., *et al.*, Effect of Package Spacing on Convective Heat Transfer from Thermal Sources Mounted on a Horizontal Surface, *Applied Thermal Engineering, 132* (2018), pp. 676–685, doi:10.1016/j.applthermaleng.2018.01.006

[18] Farhanieh, B., *et al.,* Numerical and Experimental Analysis of Laminar Fluid Flow and Forced Convection Heat Transfer in a Grooved Duct, *International Journal of Heat and Mass Transfer, 36* (1993), 6, pp. 1609–1617, doi:10.1016/s0017-9310(05)80070-5

[19] Asako, Y., and Faghri, M., Parametric Study of Turbulent Three-Dimensional Heat Transfer of Arrays of Heated Blocks Encountered in Electronic Equipment, *International Journal of Heat and Mass Transfer, 37* (1994), 3, pp. 469–478, doi:10.1016/0017-9310(94)90081-7

[20] Molki, M., and Fagri, M., Temperature of In-Line Array of Electronic Components, *Electron Cooling, 6* (2000), 2, pp. 26–32

[21] Nakayama, W., and Park, S. H., Conjugate Heat Transfer from a Single Surface-Mounted Block to Forced Convective Air Flow in a Channel, *Journal of Heat Transfer, 118* (1996), 2, pp. 301–309, doi:10.1115/1.2825845

[22] Kurşun, B., and Sivrioğlu, M., Heat Transfer Enhancement Using U-Shaped Flow Routing Plates in Cooling Printed Circuit Boards, *Journal of the Brazilian Society of Mechanical Sciences and Engineering, 40* (2018), 1, doi:10.1007/s40430-017-0937-z

[23] Bahiraei, M., *et al.*, Employing Elliptical Pin-Fins and Nanofluid within a Heat Sink for Cooling of Electronic Chips Regarding Energy Efficiency Perspective, *Applied Thermal Engineering, 183*,(2021), p. 116159, doi:10.1016/j.applthermaleng.2020.116159

[24] Bahiraei, M., and Mazaheri, N., Application of an Ecofriendly Nanofluid Containing Graphene Nanoplatelets inside a Novel Spiral Liquid Block for Cooling of Electronic Processors, *Energy (Oxford, England), 218* (2021), p. 119395, doi:10.1016/j.energy.2020.119395

[25] Bouzennada, T., *et al.*, Numerical Simulation of Heat Transfer and Melting Process in a NEPCM: Using New Fin Shape, *International Communications in Heat and Mass Transfer, 143* (2023), p. 106711, doi:10.1016/j.icheatmasstransfer.2023.106711

[26] Saeed, A. M., *et al.*, A Numerical Investigation of a Heat Transfer Augmentation Finned Pear-Shaped Thermal Energy Storage System with Nano-Enhanced Phase Change Materials, *Journal of Energy Storage, 53* (2022), p. 105172, doi:10.1016/j.est.2022.105172

[27] Mourad, A., *et al.,* Numerical Investigation of a Snowflake-Shaped Fin-Assisted Latent Heat Storage System Using Nanofluid, *Journal of Energy Storage, 55* (2022), p. 105775, doi:10.1016/j.est.2022.105775

[28] Belazreg, A., *et al.*, Insight into Latent Heat Thermal Energy Storage: RT27 Phase Transition Material Conveying Copper Nanoparticles Experiencing Entropy Generation with Four Distinct Stepped Fin Surfaces, *International Journal of Thermofluids, 19* (2023), p. 100368, doi:10.1016/j.ijft.2023.100368

[29] Mourad, A., *et al.*, Numerical Study on N-Octadecane PCM Melting Process inside a Pear-Shaped Finned Container, *Case Studies in Thermal Engineering, 38* (2022), p. 102328, doi:10.1016/j.csite.2022.102328

[30] Khaliq, A., Thermodynamic Optimization of Laminar Viscous Flow under Convective Heat Transfer through an Isothermal Walled Duct, *Applied Energy, 78* (2004), pp. 289–304

Received: 08.09.2023.
Revised: 24.01.2024.
Accepted: 27.01.2024.